INTERPRETATION OF VLF PHASE DATA

Friedrich Reder and James Hargrave
U. S. Army Electronics Technology and Devices Laboratory

James Crouchley
University of Queensland
Australia

1.0 INTRODUCTION

VLF phase tracking finds application in:

- Long-range standard frequency distribution
- Long-range clock synchronization
- Global radio navigation
- Global monitoring of the lower ionosphere and of solar activity
- Prospecting for mineral deposits

Correct interpretation of VLF phase data requires thorough training of equipment operators and data analysts since the recorded data are strongly dependent on proper equipment performance and on the interaction of all parameters describing the status of the lower ionosphere and of the ground along the path of signal propagation. Furthermore, recorded data depend on path length and signal frequency.

It is the purpose of this report to review some additional facts on the subject and to augment the information presented at the third PTTI Conference.(1) The present and previous reports are based on our experience with a global VLF-tracking network established in 1965 (Project INT-VLF). The reader is assumed to be familiar with the concepts of VLF propagation and of VLF signal tracking, and is referred to the literature for background information.(2, 3, 4)

The discussion will deal with equipment; representation of VLF waves; diurnal effects and mode interference phenomena; antipodal interference; and solar flare, galactic X-ray, and geomagnetic effects.

2.0 DISCUSSION

2.1 Equipment

Many equipment problems have been discussed previously.(1) The following figures illustrate the effects of noise and of changing control settings on the signal phase and amplitude

outputs of one popular commercial VLF receiver. Of course, these effects may differ from model to model, but it is useful to alert operators and analysts to the possible existence of such phase and amplitude variations of instrumental origin.

Figure 1 shows the experimental setup for testing a receiver. The signal generator is simply another receiver whose antenna input is disconnected and whose synthesizer output provides the signal input for the receiver being tested. The blocks marked "DB" represent fixed or variable attenuators, "noise" is a source of Gaussian noise, and the diode serves as a clipping circuit (see insert in Figure 1) to convert the Gaussian noise to some resemblance of impulsive noise of atmospheric origin.

Figure 2 depicts the influence of various S/N ratios on phase (ϕ) and amplitude (A) tracks as the receiver time-constant switch (in the phase control loop) is changed from TC = 5 to 50 and 150 seconds. (The left-hand number on top of each interval gives the signal level in dB with respect to an arbitrary dB reference; the right-hand number gives the relative noise level in dB). The amplitude recording is only slightly improved by a TC increase, but the improvement in the phase record is striking. For TC = 5 sec and S/N = -10/30, the receiver lost track. At the moments marked by vertical arrows a phase step of 10 μs was introduced in the driving signal to check whether the receiver on test was still tracking the signal. It was. This suggests a useful check to test for correct tracking under conditions of low signal strength or high noise levels as evidenced by large fluctuations of the signal-strength meter; that is, to displace the phase of the reference signal by 10 μs using the

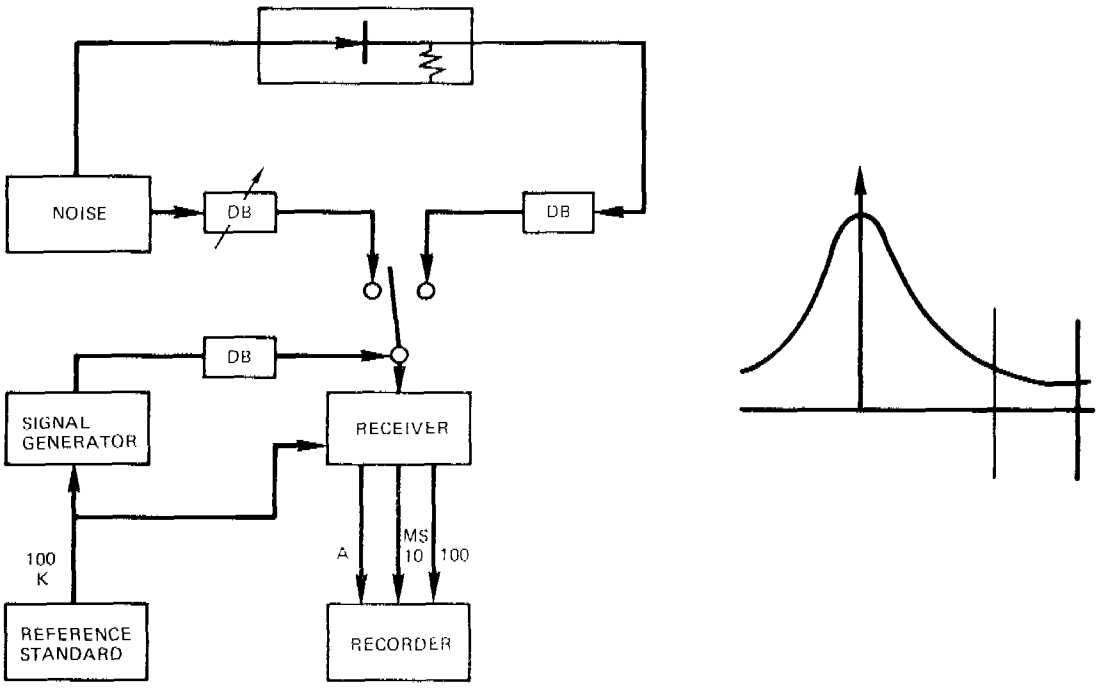

Figure 1. Block diagram of equipment set up to measure influence of S/N and equipment controls on phase and amplitude recordings.

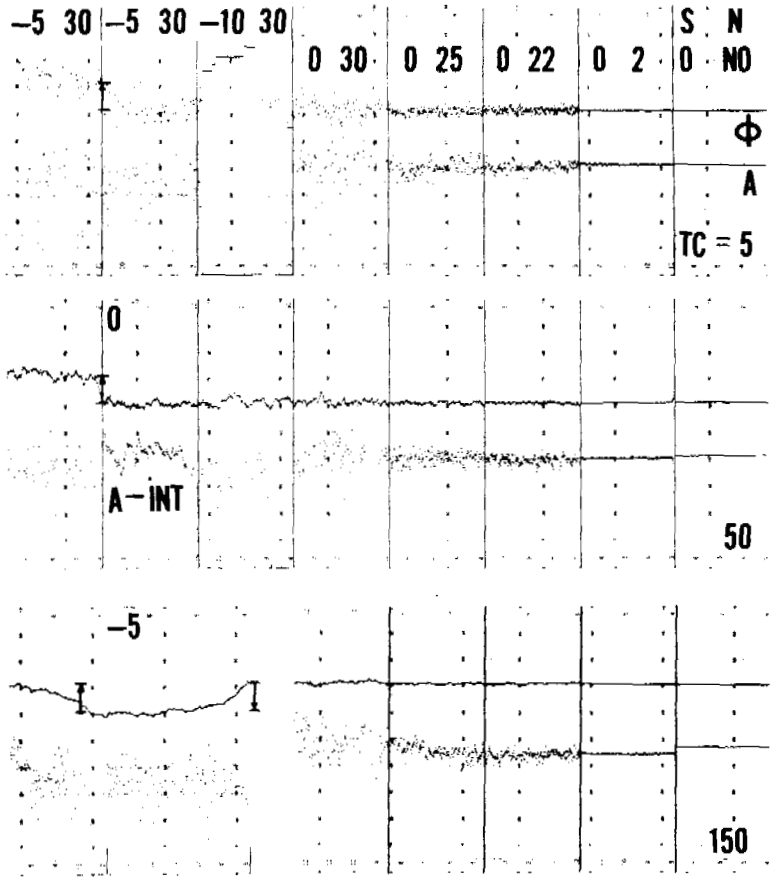

Figure 2. Influence of servo time constant, TC, and amplitude integrator on quality of phase and amplitude recordings.

slewing switch and to note if the initial phase indication is recovered. The amplitude recording for TC = 50 seconds and S/N = -5/30 was considerably improved by adding an integrator (A-INT) with a time constant of ~50 seconds at the amplitude output of the receiver. Note however that the fluctuations in this section are meaningless.

Figure 3 demonstrates the improvement of ϕ and A tracking by utilizing the blanking control of the receiver when the atmospheric noise level is high (setup of Figure 1 with noise input through the clipping diode). The blanking control is not effective with Gaussian noise.

In Figure 4 one can see that for a receiver TC = 5 seconds both the ϕ and A tracks are somewhat affected by the internal receiver noise if the signal level is reduced by 50 dB by means of an external attenuator and the receiver (internal) gain is raised by 50 dB (+50). However, internal noise would hardly be noticeable at TC = 50 seconds and larger.

The left-hand part of Figure 5 shows that the change of the TC switch causes some small

phase steps (particularly between TC = 5 and 150 seconds), but no amplitude jumps. The right-hand part reveals that changes of the electronic receiver gain are not detectable on the phase track, but that externally connected variable attenuators may be slightly reactive as evidenced by the small phase step when 10 dB attentuation was added. (If external variable attenuators are utilized for calibration, it is advisable to leave ~3 dB always in circuit in order to provide matching or else calibration readings may be in error.)

Some receiver models have synthesizer modules with an A/B switch with A for a local oscillator frequency of ($F_{SIG} + F_{IF}$), and B for ($F_{SIG} - F_{IF}$). This switch serves to increase discrimination against undesirable signals at the mirror frequency of the desired incoming signal, but the operator should be aware that changing between positions A and B may cause sizable phase and amplitude changes on the recording (Figure 6). In this connection it should be mentioned that the proper selection of the A/B switch position for interference reduction may be necessary even if the receiver has a 20 dB front-end RF filter and the

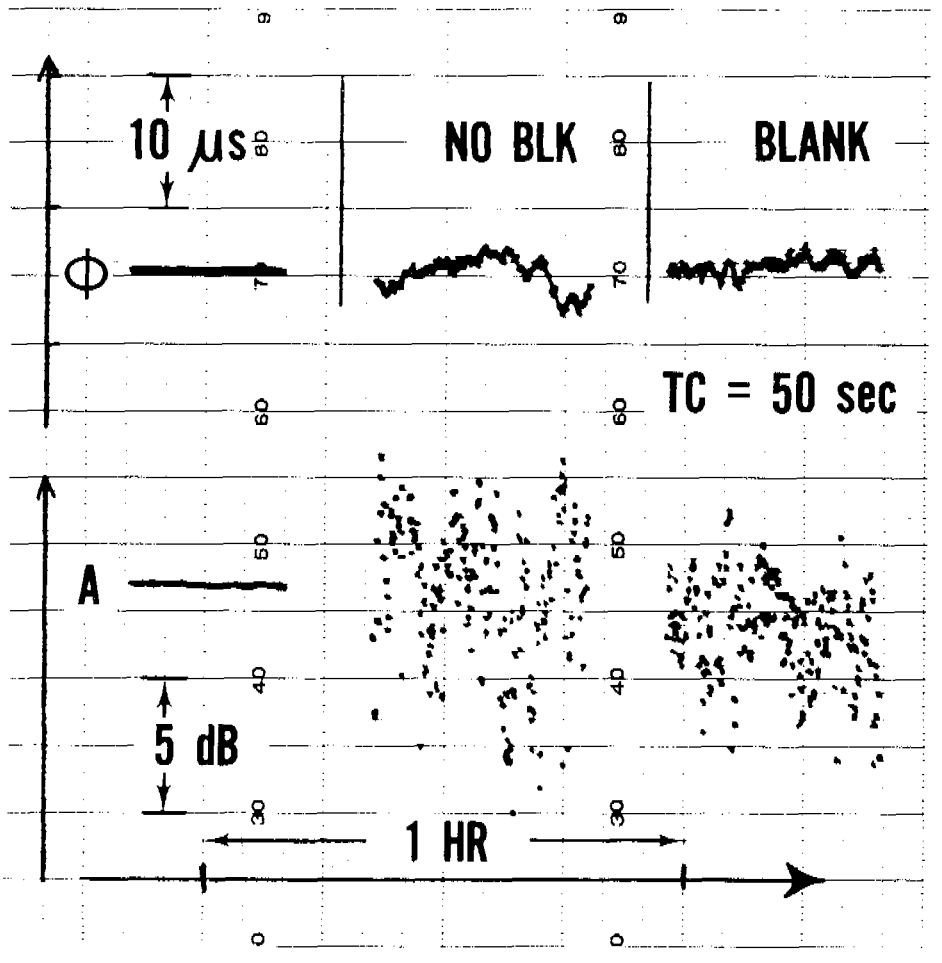

Figure 3. Effectiveness of blanking control to improve quality of phase and amplitude recordings in the presence of strong atmospheric noise.

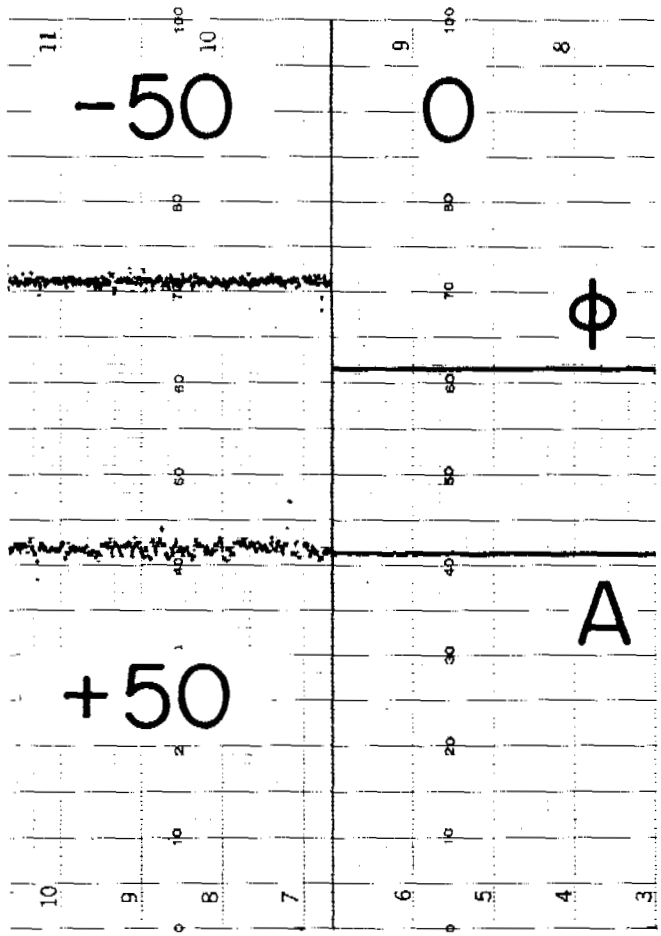

Figure 4. Effect of internal receiver noise on phase and amplitude recordings.

tuned loop antenna provides a further rejection of ~ 15 dB. For example, a Haiku-10.2 kHz receiver at Brisbane, with an IF = 1 kHz and the switch in position B (synthesizer signal at 10.2 - 1.0 = 9.2 kHz), was found to track the powerful NDT-17.4 kHz transmission with the second harmonic of the 9.2 kHz synthesizer signal (9.2 × 2 = 18.4 = 17.4 + 1 kHz). Changing to switch position A eliminated the problem. A similar problem could arise with F_{SIG} = 10.2 kHz, switch position A, and NSS (21.4 kHz) or NPM (23.4 kHz) when these transmitters are commissioned again (11.2 × 2 = 22.4 = 21.4 + 1 = 23.4 - 1 kHz).

Figure 7 depicts an experimental setup to demonstrate (Figure 8) that the coherent output from a receiver locked to a stable VLF signal and driven by a modestly-priced crystal frequency standard (e.g. internal crystal oscillator of a commercial electronic counter) can provide a 100-kHz standard reference signal of excellent accuracy to drive either a clock of microsecond precision or another VLF tracking receiver. The scope serves for a convenient adjustment of the crystal frequency to the atomically controlled frequency of a

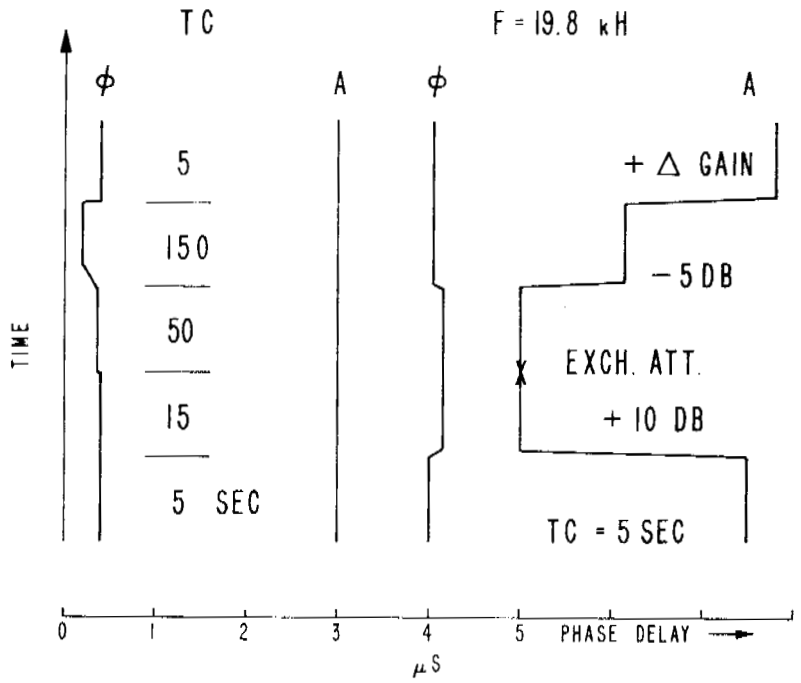

Figure 5. Phase jumps caused by changes of TC control, gain, and external attenuator settings (EXCH. ATT means external attenuator was replaced).

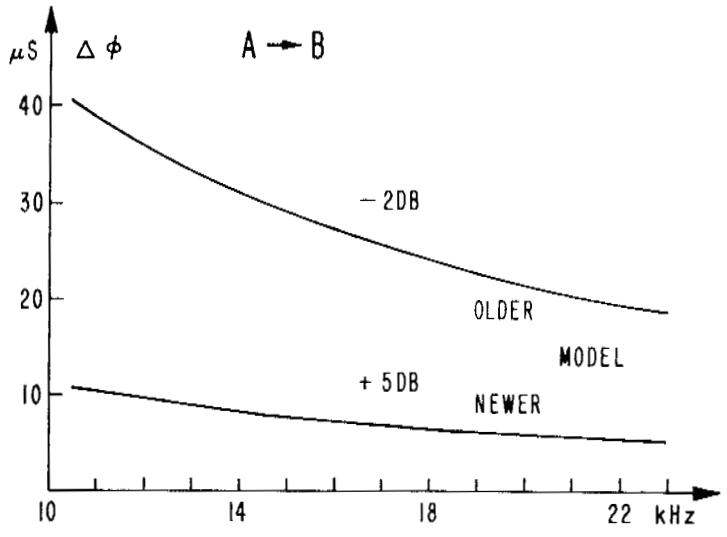

Figure 6. Phase and amplitude changes introduced by changing local reference signal from (F_S+IF) to (F_SIF). F_S is signal frequency.

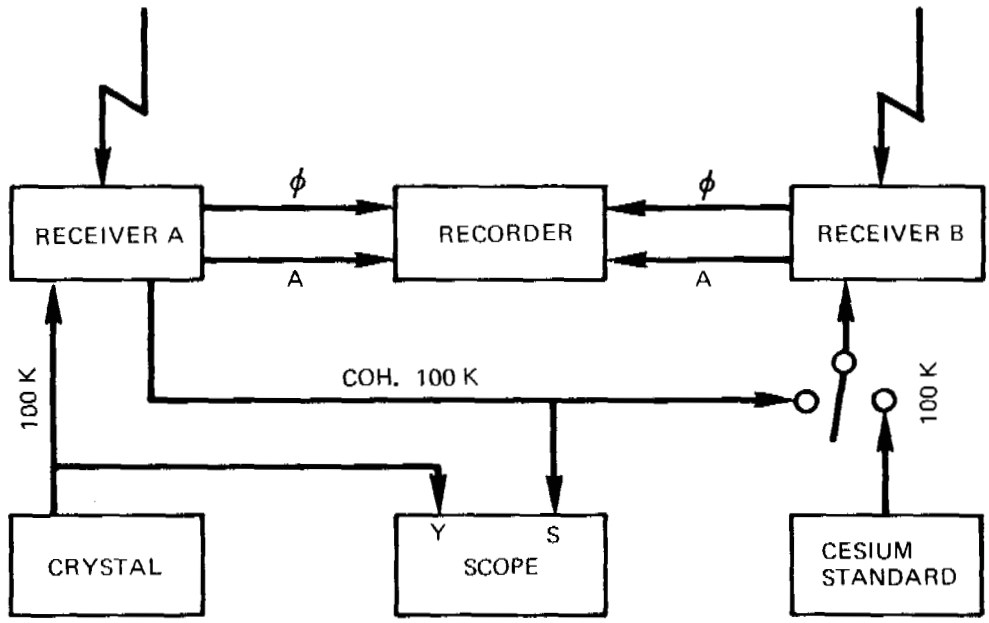

Figure 7. Block diagram for testing the usefulness of improving the accuracy of a low-cost-crystal signal by locking a VLF receiver to an atomically stabilized VLF transmission.

tracked VLF signal. The top part of Figure 8 gives the phase (lower smooth plot) and amplitude (uppermost plot) of NLK-Deal received by receiver B when driven by the 100-kHz cesium standard reference. (Time progresses to the left.) The steeply sloping lines represent the NLK-Deal phase output of the crystal-driven receiver A (crystal frequency is $\sim 5 \times 10^{-8}$ above UTC) and the middle plot is the receiver-A amplitude. It is evident that the large crystal offset does not affect the amplitude record. In the center part of Figure 8, receiver B was driven by the coherent (with NLK signal) 100-kHz output of receiver A. Since the coherent output of receiver A reproduces the diurnal shift of the NLK phase, the phase output of receiver B (100 μs full-scale at top and 10 μs full-scale at bottom) is now a horizontal line with only very small ($\sim \pm 0.2$ μs) fluctuations. Of course, the large crystal offset requires a certain phase error in the receiver in order to generate a large enough control signal to keep the receiver locked to the VLF signal. That error is larger for longer TC values of receiver A, consequently a change of the TC of receiver A changes the offset error as shown by the phase steps at the left of the figure. For TC = 150 seconds, receiver A lost track (TC values from right to left were: 50 seconds, 15 seconds [step -1.6 μs], 5 seconds [additional step of -0.6 μs], 50 seconds [back to original phase], and 150 seconds [loss of lock]). The bottom part of Figure 8 demonstrates that receiver A can provide a suitable coherent signal (provided TC_A = 5 seconds) even for a crystal offset of $\sim 24 \times 10^{-8}$ (see steep lines on right-hand side, each equivalent to a 100 μs time accumulation in $\sim$ 7 minutes). This means, that a VLF receiver driven by almost any crystal standard and locked to the VLF signal of a transmitter (preferably nearby for a small diurnal shift, e.g. NSS-Deal) can maintain synchronization of a clock to better than 5 μs. To avoid large

Table 1

Important TM Modes at Given Signal Frequencies and Distances from Transmitter for an Exponential Isotropic Ionosphere and Infinite Ground Conductivity.

F	DISTANCE (Mm)															
kHz	1	2	3	4	5	6	7	8	9	10	11	12	13	14	15	
10	1	1	1	1	1	1	1	1	1	1	1	1	1	1	1	Day
12	12	12	1	1	1	1	1	1	1	1	1	1	1	1	1	
14	12	12	1	1	1	1	1	1	1	1	1	1	1	1	1	
16	12	12	1	1	1	1	1	1	1	1	1	1	1	1	1	
18	123	12	12	1	1	1	1	1	1	1	1	1	1	1	1	
20	123	12	12	12	1	1	1	1	1	1	1	1	1	1	1	
22	213	21	12	12	12	1	1	1	1	1	1	1	1	1	1	
24	213	21	12	12	12	12	1	1	1	1	1	1	1	1	1	
26	231	21	21	12	12	12	12	1	1	1	1	1	1	1	1	
10	12	12	12	1	1	1	1	1	1	1	1	1	1	1	1	Night
12	123	12	12	12	1	1	1	1	1	1	1	1	1	1	1	
14	213	123	12	12	12	12	1	1	1	1	1	1	1	1	1	
16	213	123	21	12	12	12	12	12	1	1	1	1	1	1	1	
18	231	213	21	21	21	12	12	12	12	12	12	1	1	1	1	
20	231	231	231	21	21	21	21	21	21	12	12	12	12	12	12	
22	23	23	23	21	21	21	21	21	21	21	21	21	21	21	21	
24	23	23	23	2	2	2	2	2	2	2	2	2	2	2	2	
26	23	23	23	2	2	2	2	2	2	2	2	2	2	2	2	

clock errors when the transmitter goes temporarily off the air, it is advisable to avoid large offsets and to adjust the crystal frequency (as often as once per day) against the coherent output of receiver A.

For problems encountered with antennas, cables, battery standby supplies, connectors on receiver modules, recorders, environmental conditions for atomic frequency standards, station keeping, and transmitter interference, the reader is referred to previous publications (1, 5).

2.2 Wave Propagation (1, 2, 3, 4)

For distances less than 1 Mm it is convenient to represent the observed EM field by the following components: (6)

(a) Groundwave: not influenced by ionosphere;

(b) Ordinary skywave: vertically polarized, influenced by ionosphere; and

(c) Extraordinary skywave: horizontally polarized, influenced by ionosphere, and originating from the ordinary wave upon reflection in the ionosphere in presence of the geomagnetic field.

A whip or a long-wire antenna picks up all three components; a loop directed towards the transmitter picks up the first two components; a loop oriented precisely perpendicular to the signal path picks up primarily the last component. A separation between ground and ordinary skywave is possible by means of a whip/loop arrangement.(6) Short-path skywaves at nighttime are usually strongly disturbed in phase and amplitude due to their deeper (as compared to long-path signals) penetration into the ionosphere. The presence of the extraordinary wave causes an elliptical polarization of the skywave, reduces the depth of the "loop null," and can introduce a sizable error in direction finding by means of "loop nulling."

For distances greater than ~ 1 Mm it is advantageous to describe the EM field by modes. Each mode of order, n, is characterized by 3 parameters: excitation function Ω_n in dB, attenuation rate α_n in dB/Mm, and phase velocity V_n in units of C (velocity of light).

Mode parameters for an isotropic (no geomagnetic field) exponential ionosphere (described by a reference height h, km, and a gradient km^{-1}) and a ground of infinite conductivity (good approximation for sea water) have been published. (7, 8) Computer programs for a more sophisticated anisotropic ionosphere (because of geomagnetic field) and a ground of specified conductivity are available. (9)

Table 1 [based on Reference 8, isotropic model], shows which modes should be considered at a given signal frequency and distance. For example, 213 means that the n = 2 mode predominates over the next important n = 1 mode, and a still-weaker n = 3 mode.

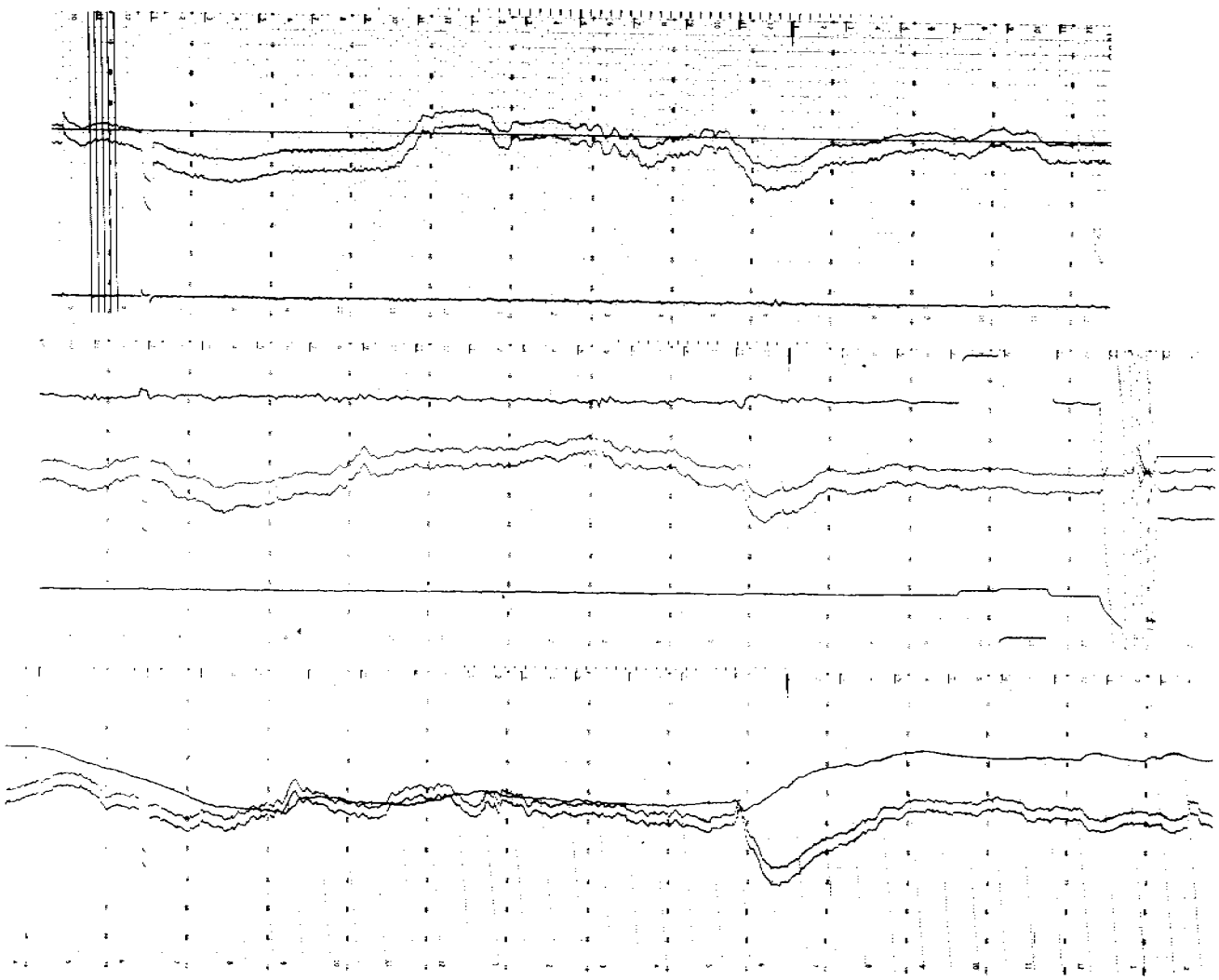

Figure 8. Demonstration of feasibility of generating precise local reference signals by phase-locking a VLF receiver, driven by a low-cost-crystal signal, to a stabilized VLF transmission.

If a VLF signal consists of two important modes with almost equal amplitudes and phase values differing by 180°, even small ionospheric changes will cause large phase fluctuations as illustrated by the phasor diagram of Figure 9. If phasor B swings further in a CCW direction with respect to phasor A, the phase deviation $\Delta\phi$ will again diminish. The plots of Figure 9 give the necessary minimum A/B ratios (in dB) for a given signal frequency in order to keep phase fluctuations due to mode interference below 1, 2, or 5 μs.

Figure 10 gives for each VLF signal frequency the minimum distance one has to be away from the transmitter in order to keep phase fluctuations, $\Delta\phi$, (as defined in Figure 9) below 1, 2, or 5 μs [based on Reference 8; h = 90 km, $\beta = 0.5$ km^{-1} for night; and h = 70 km, $\beta = 0.3$ km^{-1} for day].

The existence of the geomagnetic field gives rise to nonreciprocity of propagation losses (with reference to $\vec{NS}$, propagation losses in $\vec{EW}$ direction are larger and losses in $\vec{WE}$ direction are smaller) (3); to some variations of phase velocities as the azimuth of the path with respect to the geomagnetic field changes (10); and to the generation of TE modes and coupling between TM and TE modes. (2, 3, 9).

Low ground conductivities, as encountered in Greenland and Antarctica and somewhat less in the permafrost regions of Canada and Siberia, increase propagation losses for low ionospheric reference heights (undisturbed day, and especially during solar proton precipitations) and also affect phase velocities. (11, 12) Signal losses are also strongly increased at times when the signal path is close and nearly parallel to the solar terminator.

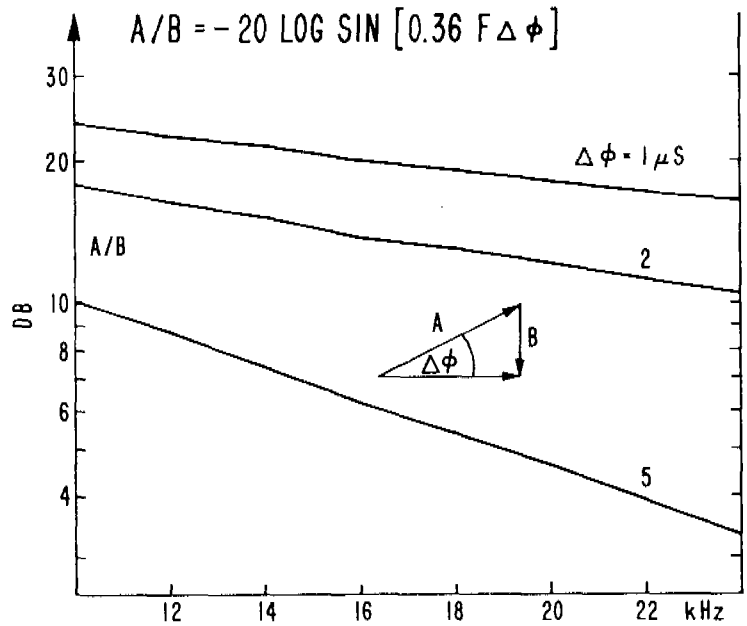

Figure 9. Maximum permissible strength B of an interfering VLF mode to keep phase anomalies due to mode interference below specified $\Delta\phi$ values at a given frequency.

2.3 Mode Interference

Values of diurnal shifts (nighttime phase is retarded with respect to daytime values) for various signal paths used in the INT-VLF Project have been quoted elsewhere.(13) Phase steps, amplitude minima and sometimes cycle slips, regularly observed during the morning hours for signal frequencies above ~ 16 kHz have been explained by Crombie (14) in terms of mode interference. Similar interference effects during the evening hours have been observed predominantly on low-latitude EW paths. (1) (15) Examples of irregular diurnal shifts observed on transequatorial paths (15) [believed to be caused by enhanced mode conversion when the terminator passes over the region where the signal crosses the geomagnetic equator (16)] may be seen in Figures 11 and 12.

The strong enhancement by mode interference of ionospheric effects on VLF phase and amplitude recordings is illustrated by the 13.6 kHz N. Dakota-Deal plots in the lower part of Figure 13 (if there were no mode interference one would expect the 10.2 kHz anomalies to be bigger than those observed at 13.6 kHz because, due to dispersion, single-mode signals are the more disturbed the lower the frequency).

The upper part of Figure 13 shows the different phase and amplitude behaviors when a signal propagating over a short distance (Forestport-Deal) is received by a loop $\parallel$ to the path (groundwave plus ordinary sky-wave) and a loop $\perp$ to the path (extraordinary wave).

2.4 Antipodal Interference

A typical example of a diurnal phase pattern obtained in the presence of antipodal signal interference (15) is shown in Figure 14. When the shorter EW path is fully sunlit, propagation losses are higher than those on the longer but nighttime WE path. Therefore, an extra hump appears during daytime along the short path.

The previously mentioned nonreciprocity of propagation losses due to the geomagnetic field extends the region of antipodal interference, in an easterly direction, from the true geographic antipode of the transmitter. Thus, signals from VLF transmitters in the U.S.A. are received at many locations in the western Pacific both along the short and long path. The geomagnetically induced nonreciprocity is so powerful that even a 14.2 kHz signal from Forestport, N.Y., was observed (15) near Guam to arrive predominantly over the long path from the west despite a path ratio of 28/12 Mm.

A peculiar antipodal interference, controlled by the large ice masses of Greenland and Antarctica, has been discussed elsewhere.(1) (15)

The effect of geomagnetic nonreciprocity on antipodal interference is enhanced if the EW path is sunlit and passes over a region of low ground conductivity. If a signal over a sunlit shorter EW path shows no signs of antipodal interference (increased phase instability, extra hump, anomalous shape of an SID) it cannot possibly show antipodal interference during nighttime along the shorter EW path. Therefore, it is unrealistic to ascribe the

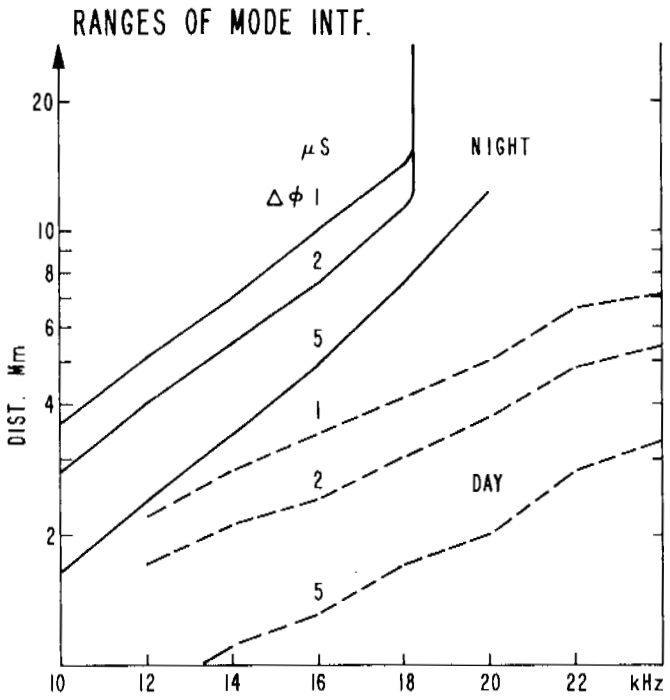

Figure 10. Minimum distances, at a given frequency, to keep mode interference effects on phase below specified limits, $\Delta\phi$. (Isotropic ionosphere.)

unusual nighttime phase behavior obtained on Haiku-Brisbane (13, 15) to antipodal interference because the short-path daytime signal reveals no evidence of such interference.

2.5 Solar Flare Effects

Solar flares cause an increased flux of X-rays and/or precipitation of electrons and/or protons in the ionosphere, giving rise to phase advances and signal amplitude changes of single-mode VLF signals.(1, 13) On short-distance signals (e.g. Forestport-13.6 kHz-Deal) composed of at least two modes and on long-distance signals affected by antipodal interference (e.g. GBR-Brisbane), phase anomalies may be reversed (delay).(1)

Solar X-ray effects (SID's) can only be observed on sunlit paths. They are detectable at all latitudes but predominantly on paths with a low-average solar zenith angle. The phase anomalies increase with illuminated path length and decreasing frequency.

In general, signal amplitude increases during an X-ray flare for signal frequencies above 16 kHz but signal decreases have been observed on GBR (16.0 kHz) and NAA (17.8 kHz) to Beirut and Tananarive during strong flares. Examples additional to those in reference (11) are shown in Figure 15. Note that GBR-Cordoba (Argentina) always experienced signal enhancements, while the strong flare on July 25, 1425 UT caused a signal decrease on NAA-TAN.

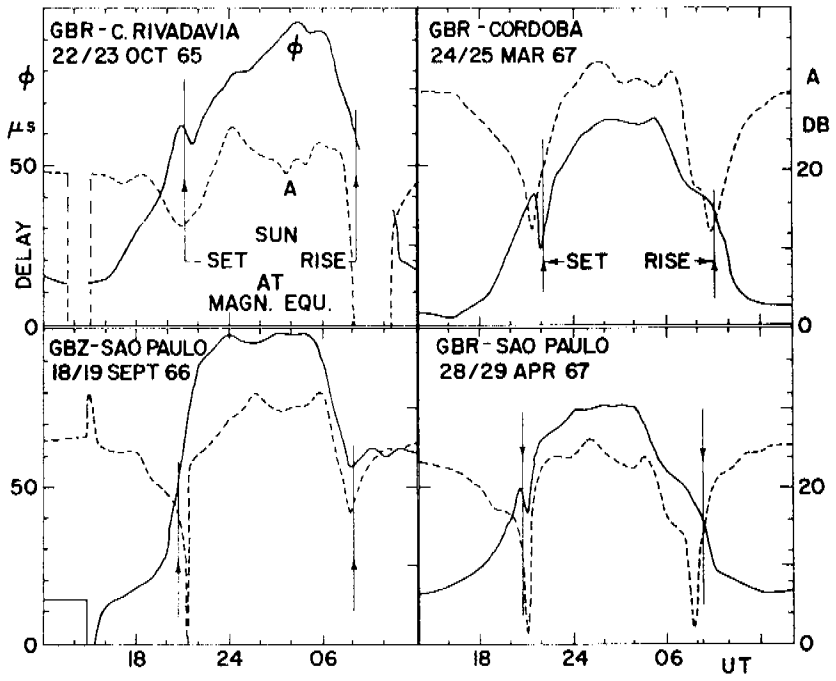

Figure 11. Examples of anomalies observed during sunrise and sunset where VLF signals cross geomagnetic equator. C. Rivadavia and Cordoba are in Argentina.

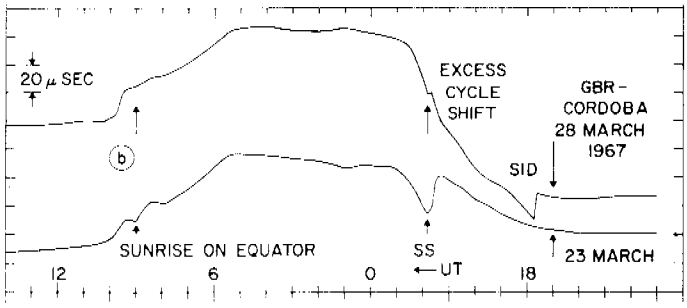

Figure 12. Another example of modal interference during sunrise and set where GBR signal crosses geomagnetic equator.

SID's usually last from 0.5 to 2 hours, in exceptional cases as long as 8 hours. Maximum deviations may be reached within a few minutes but occasionally the rise-time is as long as an hour. Maximum phase anomalies of 10 μs/Mm at 10.2 kHz have been observed a few times during 1968 and 1969.

Sometimes, the onset of a strong SID was so rapid that the receiver lost track at a TC = 50 seconds and slipped a cycle in phase. This became obvious after the ionosphere had re-

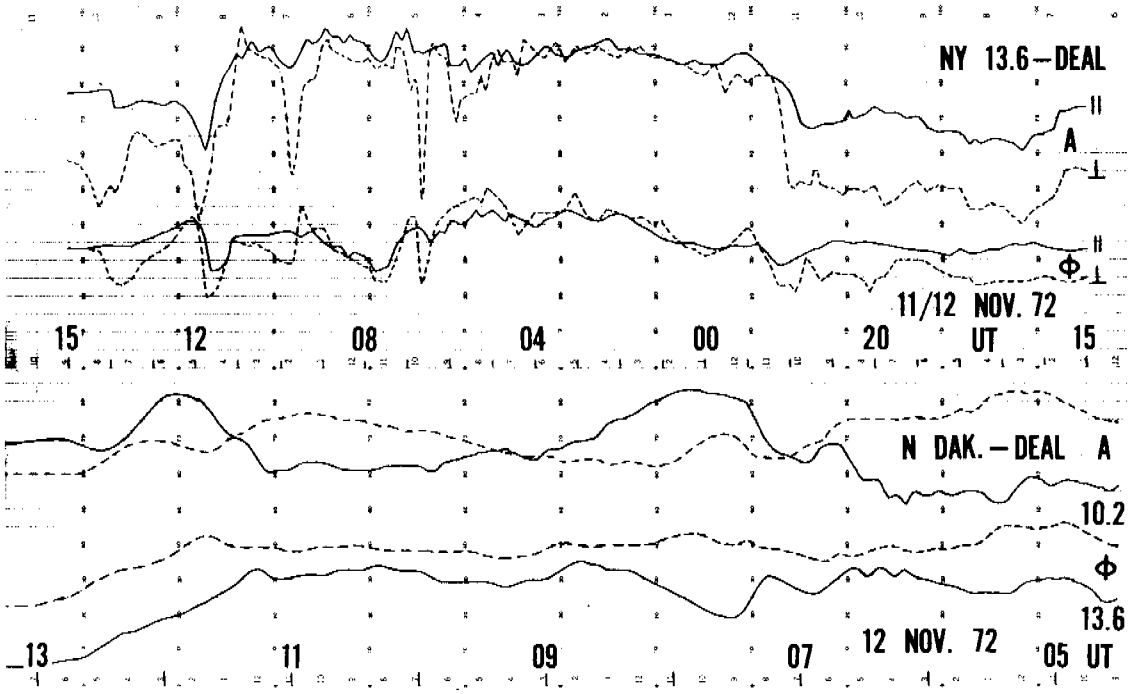

Figure 13. Difference of phase and amplitude recordings when short-distance Forestport (NY) signal is recorded with loops ∥ and ⊥ to path (top). Influence of modal interference during nighttime on N. Dakota (13.6 kHz) -Deal (NJ) transmissions (bottom).

covered and the recorded signal phase showed a delay (with respect to the phase value before SID onset) which required a correction of exactly one cycle.

VLF anomalies from electron precipitation are most frequently observed on signals passing through the auroral zone and subauroral regions.(13, 15) Electron effects are more frequently observed at night as electron energies of only about 40 keV are needed to penetrate to the nighttime reflection region (about 90 km) whereas energies of about 200 keV are needed to significantly influence the electron density in the daytime reflection region.

Electron effects typically last from one to eight hours. Figure 16 depicts some examples of electron-induced phase anomalies observed simultaneously on several signals tracked at Deal. Note the strong anomaly on the mid-latitude signal Haiku-Deal. The amplitude effects are difficult to predict. Both increases and decreases have been recorded.

Figure 17 shows a typical X-ray phase anomaly observed during daytime on NWC (22.3 kHz)-Tokyo, with a first onset at ~ 0520 UT and the dominant one at ~ 0620 UT. At ~ 0530, the signal Haiku-Deal advanced in phase. Since this path was totally in nighttime, the Haiku-Deal anomaly cannot have been due to X-rays. Furthermore, proton precipitation of such short duration is not very likely; thus electrons must be considered to be the most probable source of this disturbance.

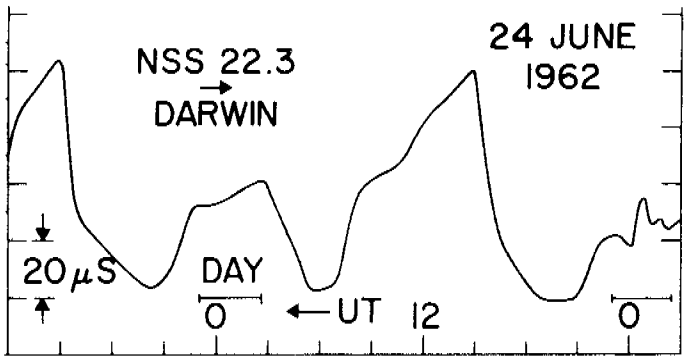

Figure 14. Example of typical antipodal interference on NSS (22.3 kHz)-Darwin (Australia).

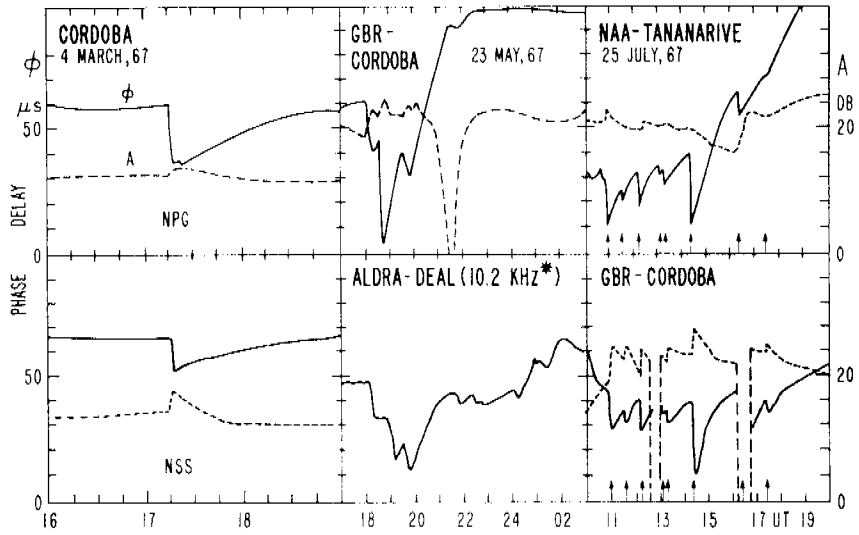

Figure 15. Examples of solar X-ray effects on long-distance VLF signals.

An interesting case of phase oscillations closely correlated with micropulsations observed by magnetometers is illustrated in Figure 18. Since oscillations of the magnetic field per se cannot affect VLF phase to that degree, the magnetic oscillations must have been accompanied by variations of the ionospheric electron density profiles. When looking at such phase oscillations, one might be tempted to suspect signal interference from another transmitter. However, signal interference requires the presence of simultaneous amplitude oscillations which are absent here. (15)

Solar proton precipitation affects the polar caps, (latitudes $>\sim 62^\circ$ geomagnetic) only, and may last from two to ten days.(1, 11) On November 28, 1968, ALDRA(10.2 kHz)-Deal showed a phase advance of $\sim 100\,\mu s$. It usually takes a few hours to reach the maximum

of the anomaly, but in this event it took only ~ 45 min. The rise time is longer if the initiating flare occurs in the eastern solar hemisphere. During simultaneous geomagnetic storms, proton effects may be noticeable down to geomagnetic latitudes of ~ 50°.

Due to the slower onset of proton anomalies one often cannot be sure whether an observed steady phase advance is caused by proton precipitation or a malfunction of the transmitter. It is easy to determine the cause if one can observe two signals of different frequencies emitted by the same transmitter (e.g. Aldra 10.2 and 13.6 kHz). If the phase traces remain exactly parallel to each other during the phase advance, it is a malfunction of the transmitter control oscillator. On the other hand, if it is a proton event, dispersion causes a more rapid phase advance at the lower frequency.

During the first few hours of an anomaly observed on a high-latitude signal one often cannot be sure whether one observes a proton or electron event. If no recovery sets in after five hours, if the phase tracks are relatively smooth, and if other signals which propagate below ~ 62° geomagnetic latitude but near the fringes of the auroral zone show no unusual anomalies, one may be fairly sure of protons. If the auroral zone signals are also disturbed and the phase behavior of the polar cap signals is not smooth, it is likely that one observes the effects of electron precipitation.

2.6 Stellar X-ray Effects

Stellar X-ray effects on VLF signals have been discussed in detail elsewhere. (17) Only the

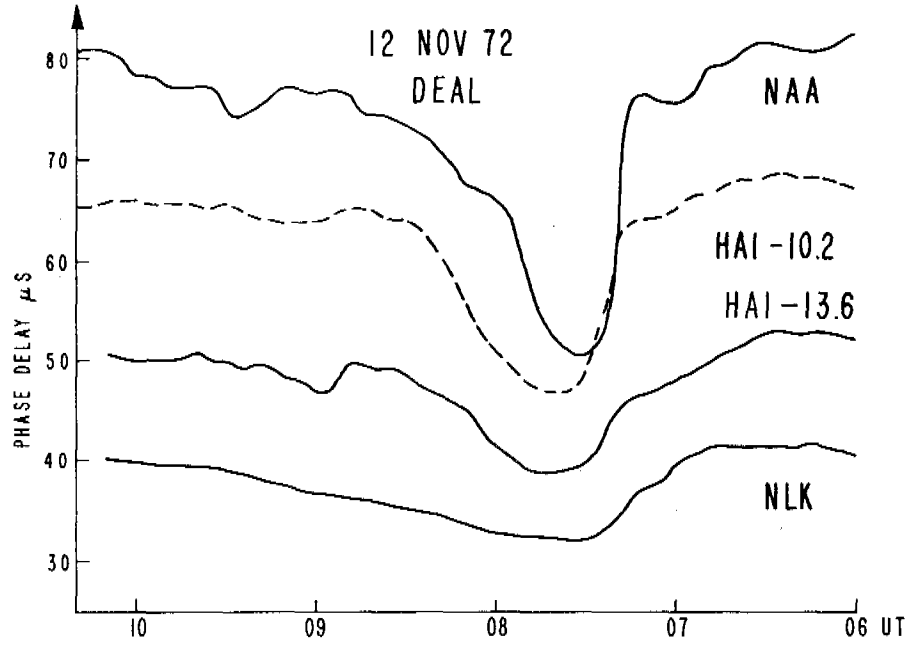

Figure 16. Examples of electron precipitation effects on VLF signals passing through subauroral regions.

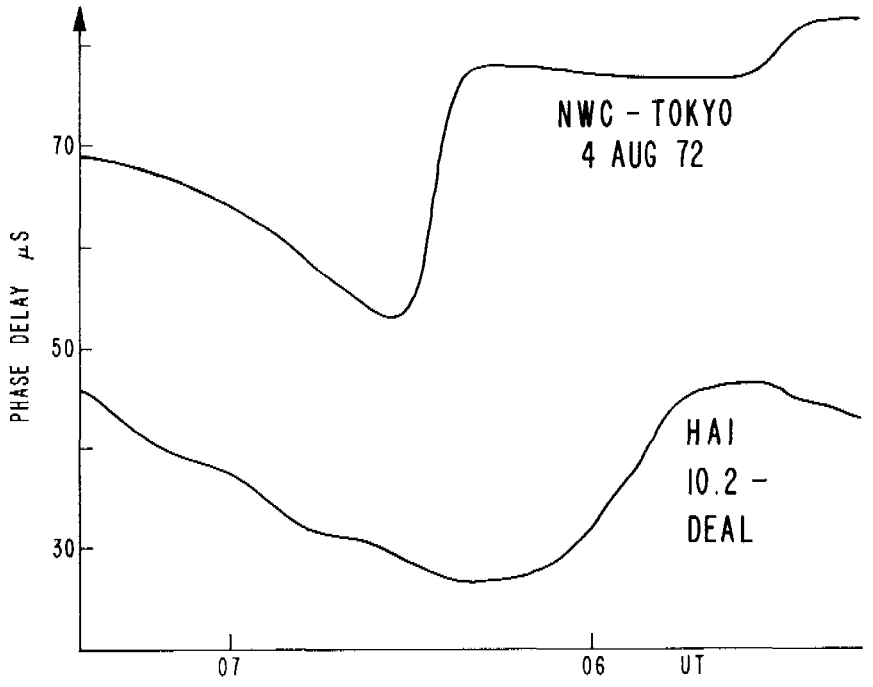

Figure 17. Example of electron precipitation effects observed on nighttime Haiku-Deal signal when daytime NWC-Tokyo showed an X-ray anomaly. It is not clear whether the correlation is accidental.

strongest stellar X-ray sources can cause a detectable phase advance during nighttime and then only provided the stellar zenith angle is very small, the night is long, and the signal frequency preferably above 20 kHz. Stellar effects must reveal a sidereal shift (occur earlier with advancing date). No detectable stellar X-ray effects were found with OMEGA navigation signals because their frequencies are well below 20 kHz.

2.7 Solar Eclipse Effects

As a solar eclipse reduces illumination along some VLF signal paths, one might expect a phase and amplitude behavior similar to that at normal nighttimes: phase delay and signal enhancement. This is illustrated by Figure 18.

3.0 CONCLUSIONS

VLF phase and amplitude tracking can be a powerful tool for frequency and time transfer, radio navigation and ionospheric monitoring provided one uses the most reliable equipment available on the market; entrusts the equipment to thoroughly trained operators; and has the data analyzed by people who are familiar with all the pitfalls of this technology and the complexity of ionospheric phenomena and multimode radio propagation.

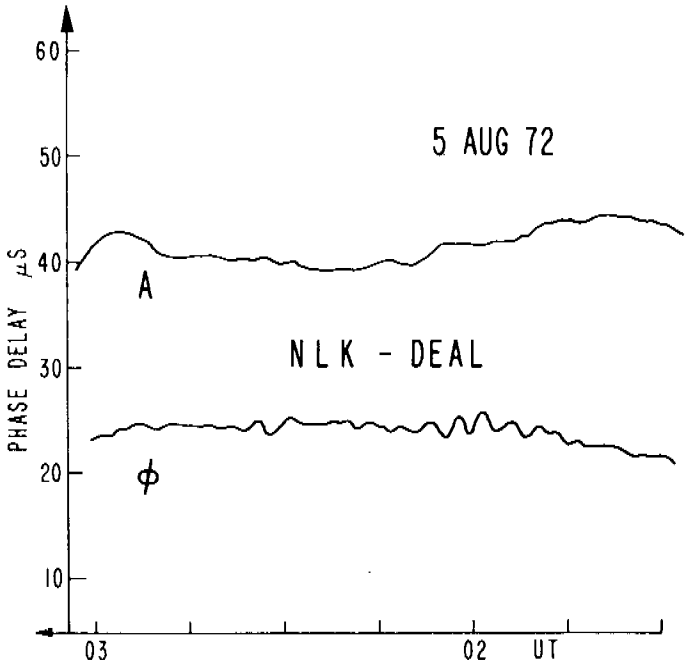

Figure 18. Example of a phase oscillation observed on NLK-Deal during period when magnetometers recorded strong micropulsations.

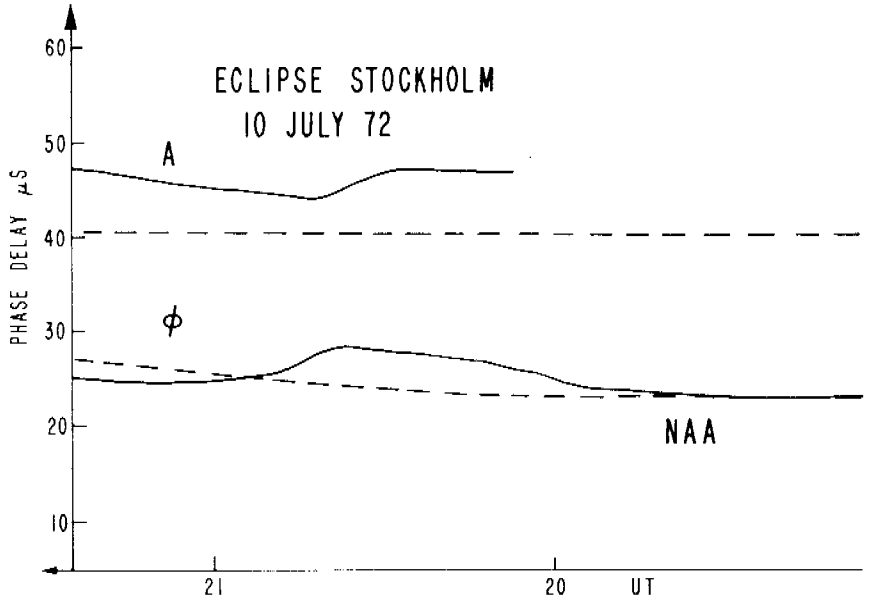

Figure 19. Phase delay and signal enhancement observed on NAA-Stockholm during solar eclipse of July 10, 1972.

ACKNOWLEDGEMENT

Some of the phase and amplitude data discussed here were provided by Col. L. Gallo of Escuella Superior de Aerotechnica, Cordoba, Argentina; Prof. P. Kaufmann, MacKenzie University, Sao Paulo, Brazil; Mr. B. Oehman, Research Institute of National Defense, Stockholm, Sweden; and Prof. R. L. Douglass, Phys. Dept., American University, Beirut, Lebanon. Figures 11 and 15 were taken from Reference 15, and Figures 12 and 14 from Reference 13.

REFERENCES

(1) F. Reder, VLF phase tracking for "precise time and time-interval" (PTTI) applications, Proc. Third PTTI Symposium, pp. 117-149, 16-18 Nov. 1971 (available from U. S. Naval Obs., Wash., D. C.).

(2) K. G. Budden, Radio Waves in the Ionosphere, Cambridge University Press, 1961.

(3) J. R. Wait, Electromagnetic Waves in Stratified Media, Pergamon Press, Oxford, 1962.

(4) A. D. Watt, VLF Radio Engineering, V. 14, International Series on Electromagnetic Waves, Pergamon Press, New York, 1967.

(5) F. Reder, Properties of VLF signals, Proc. Natl. Electronic Conf., Vol. XXVII, pp. 253-257, Oct. 9-11, 1972.

(6) R. N. Bracewell, The ionospheric propagation of radio waves of frequency 16 KC/s over distances of about 200 km, Proc. Inst. Elec. Engrs. IV, Vol. 99, pp. 217-228, 1952.

(7) J. R. Wait, K. P. Spies, Characteristics of the earth ionosphere waveguide for VLF radio waves, NBS Tech. Note 300, 1964, with 2 appendices.

(8) C. B. Brookes, J. H. McGabe, F. J. Rhoads, Theoretical VLF multimode propagation predictions, NRL Rept. 6663, 1 Dec. 1967.

(9) C. H. Sheddy, R. Pappert, Y. Gough, and W. Moler, A Fortran program for mode constants in an earth-ionosphere waveguide, Interim Rept. #683, NELC, 1968.

(10) R. J. Gallenberger, E. R. Swanson, Variations in OMEGA parameters, NELC Tech. Rept. #1773, 25 June 1971.

(11) S. Westerlund, F. Reder, C. Åbom, Effects of polar cap absorption events on VLF transmissions, Planet. Space Sci., Vol. 17, pp. 1329-1374, July 1969.

(12) S. Westerlund, F. Reder, VLF radio signals propagating over the Greenland ice-sheet, to be published in J. Atmosph. Terr. Phys., 1973 (accepted Dec 1972).

(13) F. Reder, VLF propagation phenomena observed during low and high solar activity, Prog. Radio Sci., 1966-1968, Vol. 2, pp. 113-140, URSI-Brussels, 1971.

(14) D. D. Crombie, Further observations of sunrise and sunset fading of VLF signals, Radio Sci., Vol. 1, pp. 47-51, Jan. 1966.

(15) F. Reder, S. Westerlund, VLF signal instabilities produced by propagation medium: Experimental results, AGARD Conf. Proceedings #33, pp. 103-136, Technivision Services, Slough, U.K., July 1, 1970.

(16) K. J. W. Lynn, Anomalous sunrise effects observed on a long transequatorial VLF propagation path, Radio Sci., Vol. 2, pp. 521-530, 1967.

(17) J. Svennesson, F. Reder, J. Crouchley, Effects of X-ray stars on VLF signal phase, J. Atmosph. Terr. Phys., Vol. 34, pp. 49-72, 1972.